DOI: 10.1002/chem.200700498

Highly Selective Recognition of Diols by a Self-Regulating Fine-Tunable Methylazacalix[4]pyridine Cavity: Guest-Dependent Formation of Molecular-Sandwich and Molecular-Capsule Complexes in Solution and the Solid State

Han-Yuan Gong, De-Xian Wang, Jun-Feng Xiang, Qi-Yu Zheng, and Mei-Xiang Wang*[a]

Abstract: The molecular recognition of methylazacalix[4]pyridine (MACP-4; **1**) towards various diols was investigated by using ^{1}H NMR spectroscopic and X-ray diffraction analysis. As a unique macrocyclic host molecule that undergoes conformational inversions very rapidly in solution, MACP-4 has been shown to self-regulate its conformation, through the formation of different conjugations of the four bridging nitrogen atoms with their adjacent pyridine rings, to form a cavity that best fits the guest species through intermolecular hydrogen-bond, C–H···π, and π–π interactions between the host and guest. As a consequence, depending upon the diol structure and geometry, MACP-4 forms a 1:1 molecular sandwich, 2:1 molecular capsule, and 1:2 butterfly-layered complex with the guests. As a result of favorable enthalpy and entropy effects, MACP-4 exhibits excellent selectivity in the recognition of resorcinol, thus resulting in a very stable 1:1 sandwich complex with resorcinol with a binding constant of 6000 M^{-1}. The dynamic ^{1}H NMR spectroscopic study demonstrated that the 1,3-alternate conformation of the macrocyclic ring of the MACP-4·resorcinol complex (**1·3**) is stable at low temperature ($T<$ 243 K), and its conformational inversion requires a larger activation energy ($\Delta G^{\neq} = (45.5 \pm 2.2)$ kJ mol^{-1}). In the presence of an excess amount of resorcinol, however, the conformational inversion of the MACP-4·resorcinol complex proceeds more readily with a decreased activation energy ($\Delta G^{\neq} = (33.5 \pm 1.5)$ kJ mol^{-1}) owing most probably to the favorable enthalpy effect of the [**3**···**1**···**3**]$^{\neq}$ transition state.

Keywords: host–guest systems · hydrogen bonds · methylazacalix[4]-pyridine · pi interactions · supramolecular chemistry

Introduction

Molecular recognition of diols, especially benzene diols is of great importance because many diol derivatives are naturally occurring and possess various biological properties. For example, resveratrol and epigallocatechin-3 gallate, cancer chemopreventive components found in grapes and green tea, respectively, are 1,3-benzene diol derivatives, whereas caffeic acid and epinephrine contain a 1,2-benzene diol moiety. In contrast to the achievements in the study of cation, anion, and molecular recognition by synthetic receptors,[1] the selective recognition of diols still remains challenging.[2–6] This is partly a result of the lack of efficient and selective diol receptors. In the literature, the most powerful method to recognize diols is to reversibly form boronate esters using boronic acid derivatives.[2] Besides, calix[4]resorsinol was used as a macrocyclic host to interact with aliphatic diols.[3] In a seminal paper that enabled the author to conclude that the complexation of cyclitols is strongly impeded by the intramolecular hydrogen bonds within the guest, Ansyln and co-workers[4] synthesized several polyaza clefts as receptors for cyclohexane diols and triols. However, the diol receptors reported to date show very low selectivity along with low-to-modest affinity.

Heteroatom-bridged calix(hetero)aromatic compounds[7–11] are an emerging generation of macrocyclic host molecules. Because of the different electronic nature of heteroatoms from carbon, the heteroatom-bridged calix-

[a] H.-Y. Gong, Dr. D.-X. Wang, Dr. J.-F. Xiang, Dr. Q.-Y. Zheng, Prof. Dr. M.-X. Wang
Beijing National Laboratory for Molecular Sciences
Laboratory of Chemical Biology, Institute of Chemistry
Chinese Academy of Sciences, Beijing 100080 (China)
Fax: (+86) 10-6256-4723
E-mail: mxwang@iccas.ac.cn

 © 2007 Wiley-VCH Verlag GmbH & Co. KGaA, Weinheim

(hetero)aromatic compounds exhibit intriguing and unique structural and molecular recognition properties with respect to those of the well-known calix[*n*](hetero)arenes,[12–15] in which the (hetero)arene units are linked by methylene units. For example, the introduction of oxygen and/or nitrogen atoms resulted in the formation of a number of 1,3-alternate oxa/aza-calix[2]arene[2]triazines with a fine-tuned cavity.[9a,k] On the other hand, as a result of the intrinsic nature of the bridging nitrogen atom that can adopt sp^2- and/or sp^3-electronic configurations that either conjugate or do not conjugate with the adjacent aromatic rings, azacalix[*n*]pyridines[10e] and azacalix[*m*]arene[*n*]pyridines[10d,e] have been shown to preorganize into different conformations and cavity structures so that they can interact with metal ions,[10f] anions,[10e] and fullerenes.[1d,e]

We envisioned that the multipyridine-containing feature might render methylazacalix[4]pyridine (MACP-4; **1**), a strong hydrogen-bond acceptor, able to complex diol and benzene diol derivatives through intermolecular hydrogen bonding. In addition, the aromatic rings of **1** might serve as other binding units to interact with guest species through π–π stacking and C−H···π interactions. Furthermore, the fine-tunable cavity with a defined orientation of the pyridine rings of **1** might be suitable to recognize marginally different diol and benzene diol species based on the principle of complementarity. Herein, we report the highly selective recognition of diols and benzene diols by **1** and show that it can self-regulate its conformation to form a fine-tunable cavity to include guest species. Based on the guest diol structures, **1** forms either a molecular sandwich or a molecular capsule complex with a guest both in solution and the solid state. The dynamic process of complexation of **1** with resorcinol will also be discussed.

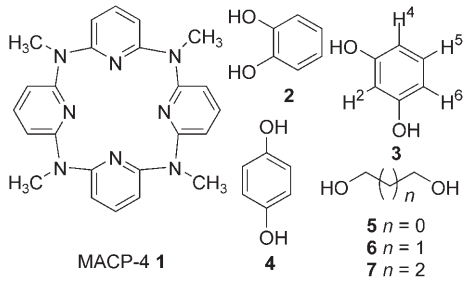

Scheme 1. Structures of host **1** and guest diols **2**–**7**.

Results and Discussion

We began our investigation with the ^{1}H NMR titration of **1**[10e] with a number of benzene diols, such as catechol (**2**), resorcinol (**3**), and hydroquinone (**4**), and aliphatic diols, including ethylene glycol (**5**), 1,3-propanediol (**6**), and 1,4-butylene glycol (**7**). As a comparison, the interaction of **1** with methanol (**8**), ethanol (**9**), propanol (**10**), and phenol (**11**) was also included (Scheme 1). As a representative of the NMR titration experiments, the spectra of a number of solutions of **3** (1.742×10^{-3} M) and **1** (0–2.316×10^{-2} M) in $CDCl_3$ at 298 K are shown in Figure 1. With an increase in the concentration of host **1**, the protons of all the guest molecules **2**–**7** gave only one set of resonance signals (see Figure 1 and the Supporting Information), thus indicating a fast equilibrium between the host, guest, and complex on the NMR timescale. Although the proton signals of the hydroxy groups of the diols showed significant downfield shift movement, all the other proton signals of the guest molecules were observed to shift upfield. Interestingly, as indicated by the Job plot experiments (see the Supporting Information), the host molecule **1** formed a 1:1 complex with all the benzene diol guests **2**–**4**, whereas the stoichiometry of the complex between **1** and the aliphatic diol **5** was 2:1. It is worth noting that as the titration of **6** and **7** with **1** gave small variations in the proton signals, no satisfactory Job plots were obtained. The 2:1 stiochiometry of complexes between **1** with

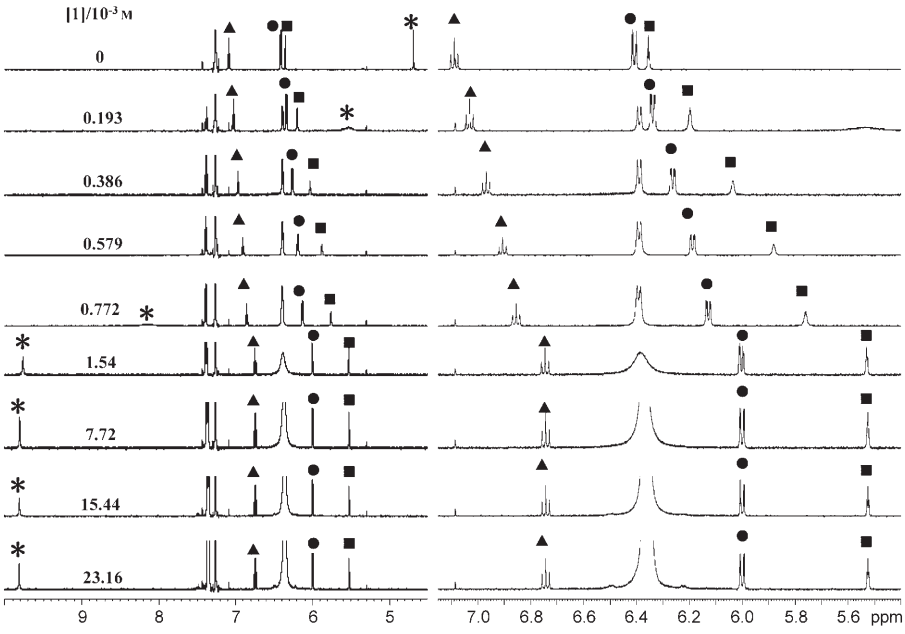

Figure 1. Left: Partial spectra of **3** (1.742×10^{-3} M) in the presence of increasing amounts of **1** (0–2.316×10^{-2} M) at 298 K. Right: Expansion of the spectra between $\delta = 5.4$ and 7.1 ppm. ■, ●, ▲, and * indicate the proton signals corresponding to H2, H4(6), and H5 on the aromatic ring and the hydroxy group of **3**, respectively.

 © 2007 Wiley-VCH Verlag GmbH & Co. KGaA, Weinheim

Table 1. Association constants (K_a) for complexation of host **1** with different guests at 298 K.

Guest	**2**	**3**	**4**	**5**	**5**	**6**	**6**
1/guest	1:1	1:1	1:1	1:1	2:1	1:1	2:1
K_a	$(1.0\pm0.0)\times10^{2}\,M^{-1}$	$(6.0\pm0.0)\times10^{3}\,M^{-1}$	$(2.5\pm0.1)\times10^{1}\,M^{-1}$	$(2.9\pm0.1)\times10^{1}\,M^{-1}$	$(3.2\pm0.0)\times10^{2}\,M^{-2}$	$(2.0\pm0.1)\times10^{1}\,M^{-1}$	$(9.3\pm0.1)\times10^{1}\,M^{-2}$

Guest	**7**	**7**	**8**	**9**	**10**	**11**
1/guest	1:1	2:1	1:1	1:1	1:1	1:1
K_a	$(1.1\pm0.1)\times10^{1}\,M^{-1}$	$(1.91\pm0.0)\times10^{2}\,M^{-2}$	$(3.0\pm0.1)\times10^{1}\,M^{-1}$	$(2.7\pm0.0)\times10^{2}\,M^{-1}$	$(4.3\pm0.1)\times10^{1}\,M^{-1}$	$(1.2\pm0.1)\times10^{1}\,M^{-1}$

Table 2. X-ray crystallographic data of the complexes between **1** and the guest molecules.

	1·**2**$_2$	**1**·**3**	**1**·**4**$_{0.5}$	**1**·**5**	**1**·**6**	**1**·**8**	**1**·**9**
	MACP-4 ·2 catechol	MACP-4·resorcinol	MACP-4·0.5 hydroquinone	MACP-4·ethylene glycol	MACP-4·1,3-propanediol	MACP-4·methanol	MACP-4·ethanol
empirical formula	$C_{35}H_{36}N_8O_4$	$C_{30}H_{45}N_8O_2$	$C_{27}H_{27}N_8O$	$C_{26}H_{30}N_8\,O_2$	$C_{27}H_{32}N_8O_2$	$C_{25}H_{28}N_8O$	$C_{26}\,H_{30}\,N_8\,O$
M_r	632.72	549.74	479.57	486.58	500.61	456.55	470.58
crystal size [mm^3]	$0.55\times0.15\times0.13$	$0.38\times0.30\times0.09$	$0.61\times0.29\times0.13$	$0.31\times0.14\times0.11$	$0.51\times0.17\times0.12$	$0.46\times0.25\times0.22$	$0.89\times0.33\times0.17$
crystal system	triclinic	monoclinic	monoclinic	monoclinic	monoclinic	monoclinic	monoclinic
space group	*C*2/*c*	*C*2/*c*	*P*2(1)/*c*	*P*2(1)/*c*	*P*2(1)/*c*	*P*2(1)/*n*	*P*2(1)/*c*
a [Å]	18.698(4)	10.4311(13)	10.615(2)	15.250(3)	15.282(3)	6.1657(12)	15.061(3)
b [Å]	9.0392(18)	20.288(3)	18.712(4)	20.738(4)	21.157(4)	18.607(4)	21.149(4)
c [Å]	19.665(4)	13.0030(14)	12.604(3)	16.373(3)	16.509(3)	20.110(4)	16.002(3)
α [°]	90.00	90.00	90.00	90.00	90.00	90.00	90.00
β [°]	96.78(3)	96.6620(18)	98.10(3)	106.12(3)	106.05(3)	91.04(3)	105.57(3)
γ [°]	90.00	90.00	90.00	90.00	90.00	90.00	90.00
V [Å^3]	3300.3(11)	2733.2(6)	2478.7(8)	4974.2(17)	5129.4(18)	2306.7(8)	4909.7(17)
d [g cm^{-3}]	1.273	1.336	1.285	1.299	1.296	1.315	1.273
Z	4	4	4	8	8	4	8
T [K]	293(2)	293(2)	293(2)	293(2)	293(2)	293(2)	293(2)
$R1$, $wR2$	0.0757	0.0493	0.0542	0.0665	0.2026	0.0747	0.0896
$I>2\sigma(I)$	0.2333	0.0942	0.1381	0.1459	0.4808	0.2208	0.2459
$R1$, $wR2$ (all data)	0.1149	0.1280	0.1289	0.1796	0.3620	0.1199	0.1522
	0.2606	0.1029	0.1610	0.1785	0.5507	0.2369	0.2689
quality of fit	1.017	0.990	0.970	1.040	1.148	1.094	1.038
CCDC no.	642301	616865	616864	616866	642300	642303	642302

6 and **7** was therefore obtained using the nonlinear least-squares fit method[16] based on the titration experiments. The association constants were calculated on the basis of ^{1}H NMR titration isotherms (see the Supporting Information) by using the Hyperquad2003 program[17] (Table 1).

Although **1** was able to complex various diols, its binding ability and binding model, however, varied dramatically depending on the structure of the diol guest. As revealed by the data complied in Table 1, **1** formed a 2:1 complex with aliphatic diols **5**–**7**, thus giving association constants of 320, 93, and 191 M^{-2}, respectively. Intriguingly, in the case when a 1:1 complex was formed, the strongest interaction was observed between **1** and **3** with an association constant of 6000 M^{-1}, followed by the complexation of **1** with **9** (K_a = 270 M^{-1}) and **2** (K_a = 100 M^{-1}). The 1:1 binding of **1** with all the other diols and monools tested was weak and the binding constants ranged only from 11 to 43 M^{-1}.

The observations of the downfield shift movement of the hydroxy proton signals and the shielding effect of the rest of the proton resonances of the diol in the ^{1}H NMR titration experiments upon the addition of **1** suggested, respectively, intermolecular hydrogen bonding and the formation of an inclusion complex between the host and guest. To obtain direct evidence and, more importantly, to understand the driving forces or the nature of the interactions in the complexation between the host and guest, single crystals of the complexes were cultivated. Gratifyingly, the interaction of **1** under the appropriate conditions (see the Experimental Section) with **2**–**6**, **8**, and **9** gave high-quality single crystals of the corresponding complexes and their structures were determined by X-ray crystallographic studies (Table 2).

The results depicted in Figures 2–8 illustrate several remarkable structural features of the complexes in the solid state. First of all, interaction of **1** with a guest led to more complexation patterns in the solid state than in the solution phase. Whereas only 1:1 and 2:1 complexations between **1** and different guests were observed in solution, complexes with three different stoichiometries were formed in the solid state. Except for the methanol·MACP-4 "complex" (**1**·**8**), in which **8** did not interact with **1** (Figure 7), the interaction of **1** with **3**, **5**, **6**, and **9** (Figures 3, 5, 6, and 8, respectively) all gave 1:1 sandwich-type complexes, whereas complexation between **1** and **4** (Figure 4) and **2** (Figure 2) gave rise to a 2:1 capsule-like complex and a 1:2 butterfly-layered com-

 © 2007 Wiley-VCH Verlag GmbH & Co. KGaA, Weinheim

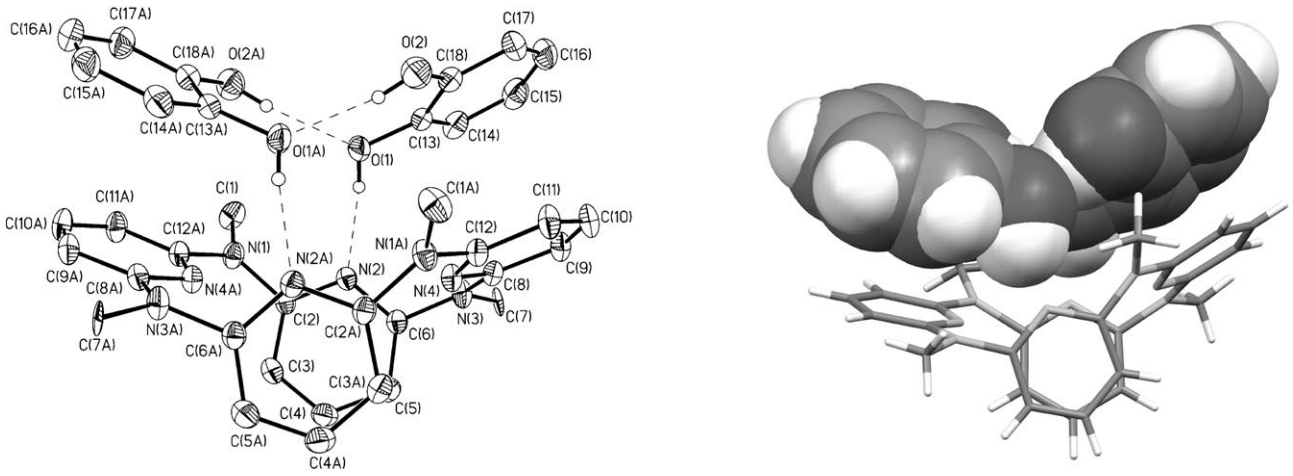

Figure 2. Molecular structure of the MACP-4·catechol complex **1**·2_2. Selected interatomic distances [Å]: N(2)···N(2A) 4.538, C(4)···C(4A) 3.915, N(4)···N(4A) 4.869, C(10)···C(10A) 9.921, N(2)···N(4) 2.968, N(4)···N(2A) 3.654, N(2 A)···N(4A) 2.968, N(4 A)···N(2) 3.654, N(4)···C(13) 3.448, C(8)···C(14) 3.454, C(9)···C(15) 3.667, C(10)···C(16) 3.877, C(11)···C(17) 3.845, C(12)···C(18) 3.627. Selected bond lengths [Å]: N(1)−C(2) 1.417, N(1)−C(12) 1.385, N(3)−C(8) 1.375, N(3)−C(6) 1.429, N(1A)−C(2A) 1.417, N(1A)−C(12A) 1.385, N(3A)−C(8A) 1.375, N(3A)−C(6A) 1.429, O(1)−N(2) 2.715 O(1A)−N(2A) 2.715, O(2)−O(1A) 2.819, O(1)−O(2A) 2.819. Selected bond angles [°]: O(1)-H(1G)-N(2) 165.09, O(1B)-H(1GB)-N(2B) 165.09, O(2)-H(2B)-O(1B) 153.96, O(2B)-H(2BB)-O(1) 153.96.

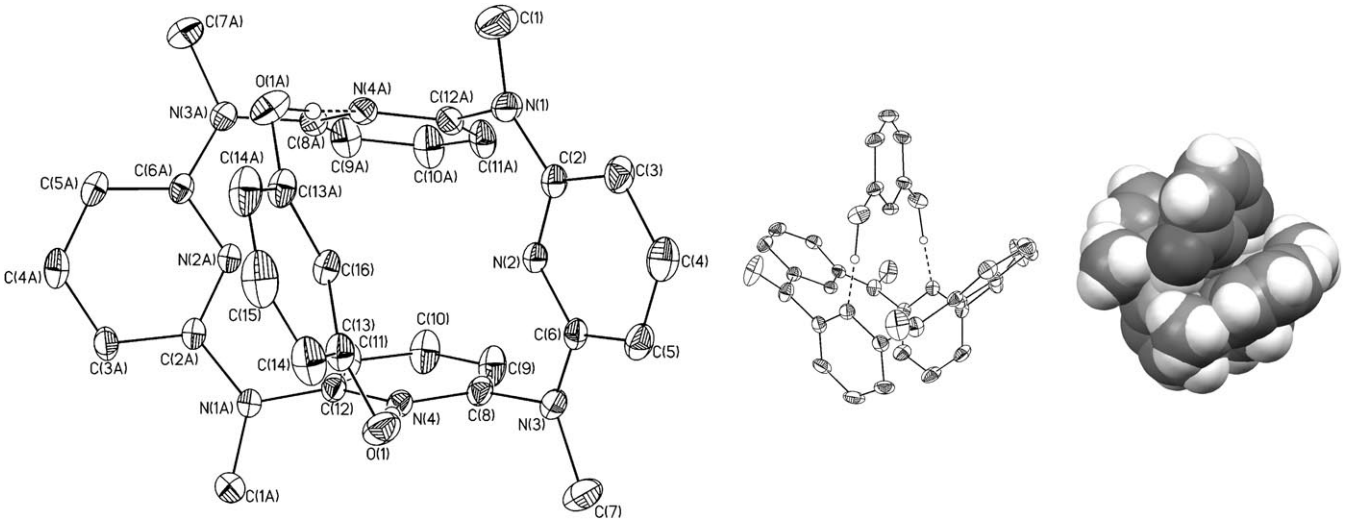

Figure 3. Molecular structure of MACP-4·resorcinol complex **1**·**3**. Left: top view; middle and right: side views. Selected interatomic distances [Å]: N(2)···N(2A) 4.822, C(4)···C(4A) 9.084, N(4)···N(4A) 4.530, C(10)···C(10A) 3.416, N(2)···N(4) 3.124, N(4)···N(2A) 3.448, N(2 A)···N(4A) 3.124, N(4A)···N(2) 3.448. Selected bond lengths [Å]: N(1)−C(2) 1.383, N(1)−C(12) 1.400, N(3)−C(6) 1.376, N(3)−C(8) 1.419, N(1A)−C(2A) 1.383, N(1)−C-(12A) 1.400, N(3A)−C(6A) 1.376, N(3A)−C(8A) 1.419, N(2)−C(16) 3.477, O(1)−N(4) 2.748, O(1A)−N(4A) 2.748. Selected bond angles [°]: O(1)-H(1)-N(4) 177.05, O(1 A)-H(1 A)-N(4) 177.05.

plex, respectively. Second, in all cases, macrocyclic host **1** adopted a 1,3-alternate conformation or a slightly twisted 1,3-alternate conformation with two isolated pyridine rings almost face-to-face in parallel and with the other two conjugated 2,6-bis(methylamino)pyridine segments edge-to-edge orientated. In addition, in each complex, noticeably, attributable to electronic effects, the nitrogen atoms of two isolated pyridine rings rather than of the conjugated 2,6-bis(methylamino)pyridine components acted as the acceptors to form intermolecular hydrogen bond(s) with the hydroxy group(s) of the guest. The distances between the hydrogen-bond acceptor and donor (d(N···O)) ranged from 2.656 to 3.133 Å, and the hydrogen-bond angles (∢O−H···N) were in the range 132.60–177.05° (see the legends of Figures 2–8). Two conjugated 2,6-bis(methylamino)pyridine segments, on the other hand, formed a cavity or a cleft to accommodate the guest.

Furthermore, it is worth noting that in addition to the intermolecular hydrogen bonding careful scrutiny of the molecular structures also revealed C−H···π interactions between one of the methylene groups of the ethylene glycol and the two edge-to-edge orientated pyridine rings in the

 © 2007 Wiley-VCH Verlag GmbH & Co. KGaA, Weinheim

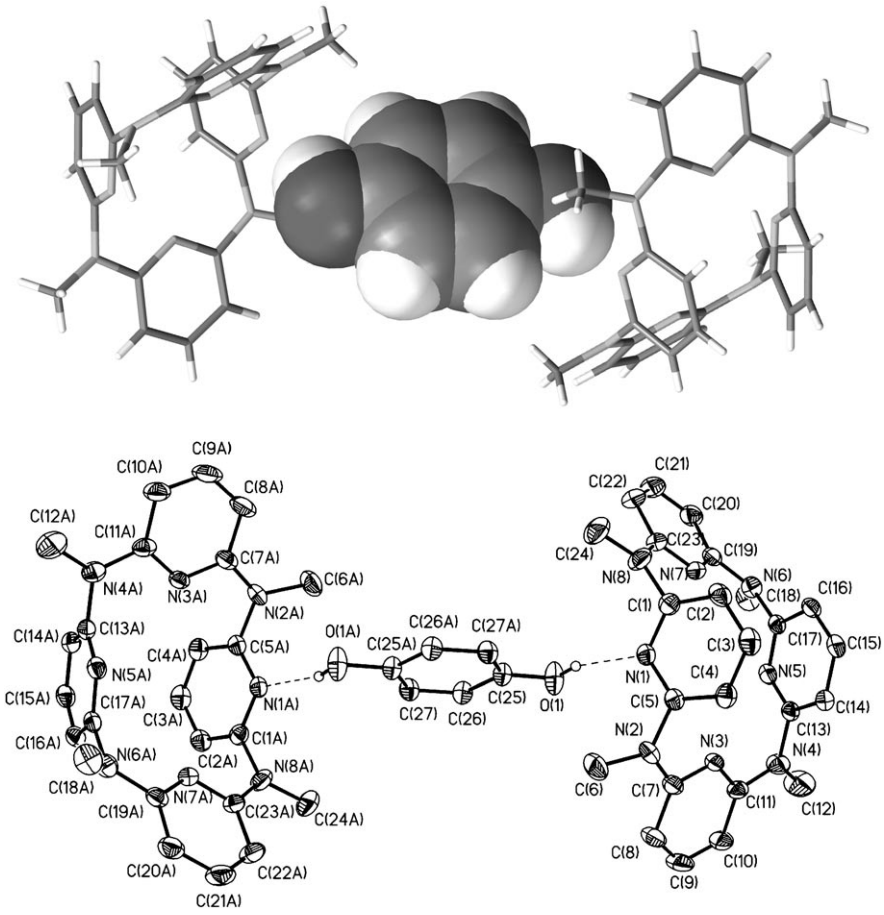

Figure 4. Molecular structure of MACP-4·hydroquinone complex $\mathbf{1}_2$·**4** (side views). Selected interatomic distances [Å]: N(1)···N(5) 4.644, C(3)···C(15) 3.439, N(3)···N(7) 4.852, C(9)···C(21) 9.669, N(1)···N(3) 3.411, N(3)···N(5) 3.304, N(5)···N(7) 3.440, N(7)···N(1) 3.282. Selected bond lengths [Å]: C(5)–N(2) 1.422, N(2)–C(7) 1.376, C(11)–N(4) 1.373, N(4)–C(13) 1.428, C(17)–N(6) 1.411, N(6)–C(19) 1.405, C(23)–N(8) 1.382, N(8)–C(1) 1.423, O(1)–N(1) 2.748. Selected bond angles [°]: O(1)-H(1)-N(4) 177.05.

MACP-4·ethylene glycol complex (**1·5**), as the distances between the H(49A) and N(7) and H(49B) and N(3) atoms are 2.785, and 2.789 Å, respectively (Figure 5). Similar C–H···π interactions were also seen in the MACP-4·1,3-propanediol (**1·6**) and MACP-4·ethanol (**1·9**) complexes. The distances between the H(49A) and N(7) and H(49B) and N(3) atoms are 2.785 and 2.789 Å, respectively (Figures 6 and 8). Moreover, in the case of the 1:2 complex between **1** and **2**, there are strong π–π stacking interactions between each of the edge-to-edge orientated pyridine rings and one of the catechol rings, in addition to a network of intermolecular hydrogen bonds between the host and two guest molecules. The distance between the pyridine and benzene rings is 3.225–3.609 Å (Figure 2).

Finally, it is very important to address that although **1** adopted a 1,3-alternate or a slightly twisted 1,3-alternate conformation in all the complexes, depending on which guest molecule was included, the bond lengths between the bridging nitrogen atoms and their adjacent pyridine carbon atoms

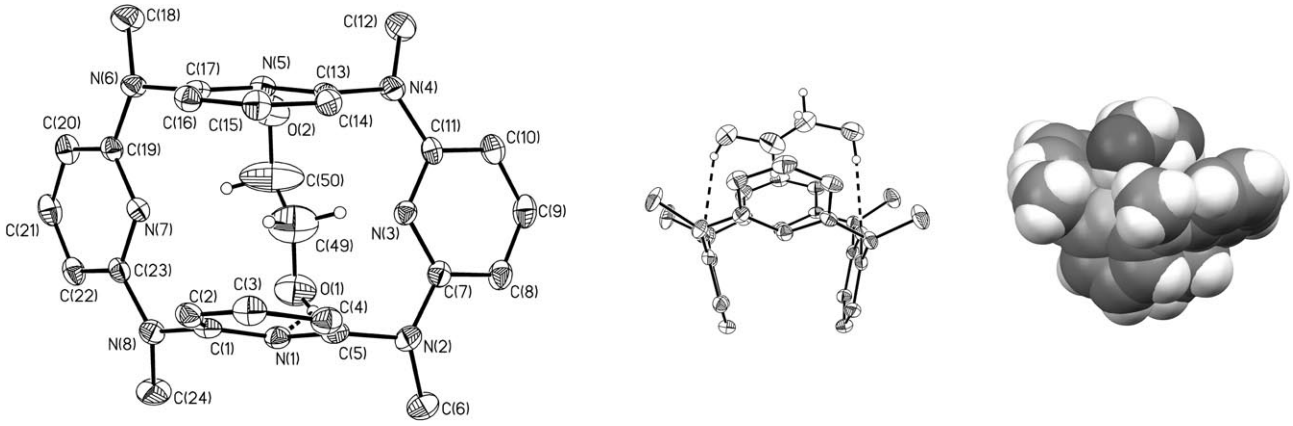

Figure 5. Molecular structure of MACP-4·ethylene glycol complex **1·5**. Only one complex structure in the crystallographic cell is shown. Left: top view; middle and right: side views. Selected interatomic distances [Å]: N(1)···N(5) 4.605, C(3)···C(15) 3.416, N(3)···N(7) 4.881, C(9)···C(11) 9.188, N(1)···N(3), 3.248, N(3)···N(5) 3.460, N(5)···N(7) 3.229, N(7)···N(1) 3.482, HA(C49)···N(7) 2.785, HB(C49)···N(3) 2.789. Selected bond lengths [Å]: C(5)–N(2) 1.431, N(2)–C(7) 1.380, C(11)–N(4) 1.385, N(4)–C(13) 1.423, C(17)–N(6) 1.437, N(6)–C(19) 1.388, C(23)–N(8) 1.382, N(8)–C(1) 1.421, O(1)–N(1) 3.004, O(2)–N(5) 2.966. Selected bond angles [°]: O(1)-H(1A)-N(1) 132.60, O(2)-H(2B)-N(5) 168.84.

 © 2007 Wiley-VCH Verlag GmbH & Co. KGaA, Weinheim

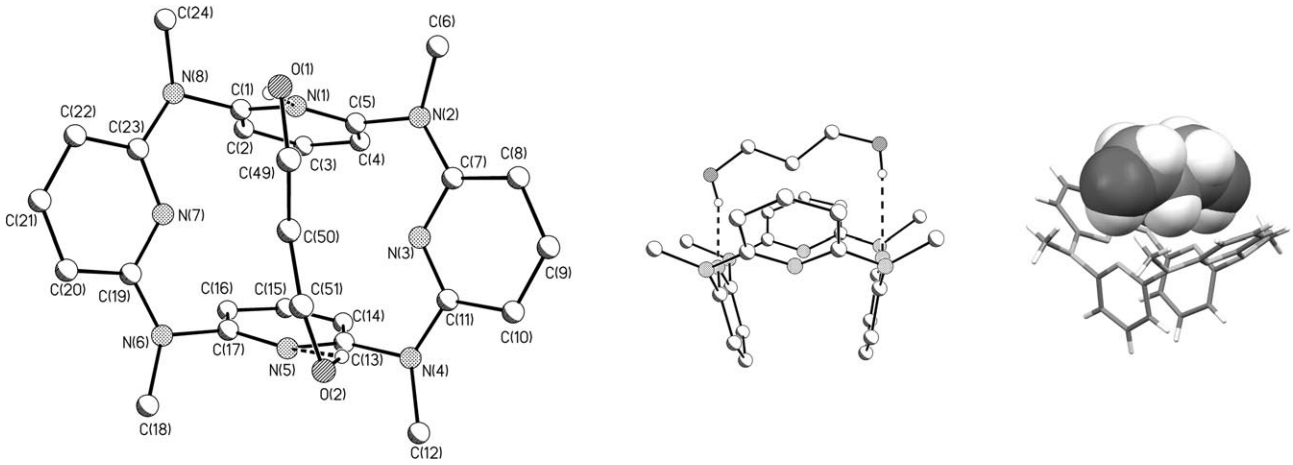

Figure 6. Molecular structure of MACP-4·1,3-propanediol complex **1·6**. Only one complex structure in the crystallographic cell is shown. Left: top view; middle and right: side views. Selected interatomic distances [Å]: N(1)···N(5) 4.566, C(3)···C(15) 3.372, N(3)···N(7) 4.838, C(9)···C(11) 8.989, N(1)···N(3), 3.396, N(3)···N(5) 3.244, N(5)···N(7) 3.440, N(7)···N(1) 3.228, O(1)···N(1) 3.132, O(2)···N(5) 2.731, HA(C50)···N(7) 2.709, HB(C50)···N(3) 2.621. Selected bond lengths [Å]: C(5)–N(2) 1.421, N(2)–C(7) 1.359, C(11)–N(4) 1.393, N(4)–C(13) 1.460, C(17)–N(6) 1.428, N(6)–C(19) 1.356, C(23)–N(8) 1.381, N(8)–C(1) 1.448, N(3)–H(50B) 2.621, N(7)–H(50A) 2.709, O(1)–N(1) 3.132. Selected bond angles [°]: O(1)-H(1A)-N(1) 155.54, O(2)-H(2B)-N(5) 127.49.

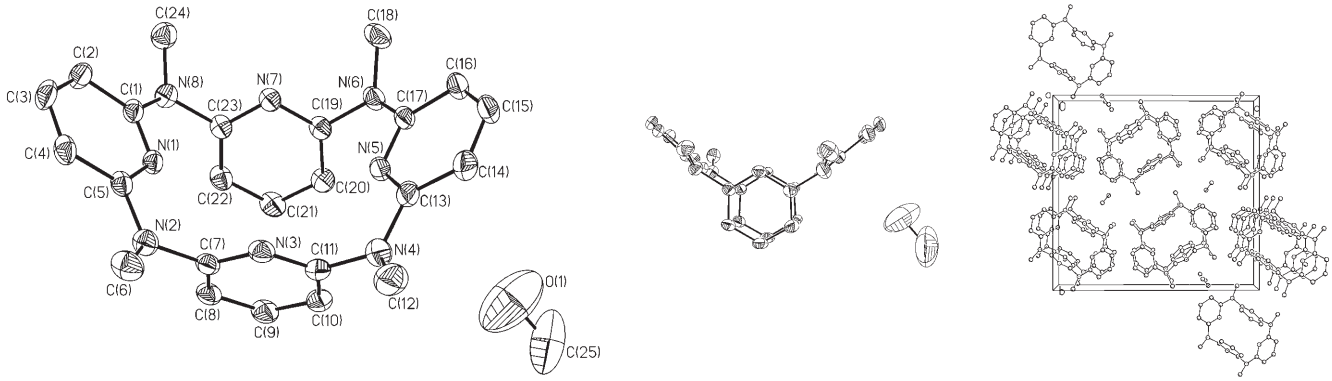

Figure 7. Molecular structure of MACP-4·methanol complex **1·8**. Selected interatomic distances [Å]: N(1)···N(5) 4.832, C(3)···C(15) 9.014, N(3)···N(7) 4.622, C(9)···C(21) 3.308, N(1)···N(3), 3.389, N(3)···N(5) 3.326, N(5)···N(7) 3.377, N(7)···N(1) 3.297. Selected bond lengths [Å]: C(5)–N(2) 1.377, N(2)–C(7) 1.439, C(11)–N(4) 1.431, N(4)–C(13) 1.397, C(17)–N(6) 1.389, N(6)–C(19) 1.431, C(23)–N(8) 1.438, N(8)–C(1) 1.385.

varied slightly (see the legends for Figures 2–8), thus leading to various fine-tuned cavity sizes. For example, the cavity, which was defined by the upper-rim distance between two edge-to-edge positioned pyridine rings, gradually increased from 9.014 (parent **1**), 9.084 (**1·3**), 9.188–9.359 (**1·5**), 9.669 (**1_2·4**) to 9.921 Å (**1·2_2**). On the other hand, the lower-rim distance between two face-to-face parallel pyridine rings, that is, the distance between two hydrogen-bond acceptors, ranged from 4.530 (**1·3**), 4.538 (**1·2_2**), 4.566–4.591 (**1·6**), 4.591–4.605 (**1·5**), 4.622 (parent **1**), 4.630–4.642 (**1·9**) to 4.644 Å (**1_2·4**).

The ability of **1** to form different types of complexes with diols and monools in the solid state is remarkable and is most probably determined by, or originates from, the unique macrocyclic nature of **1**. Compound **1** is a fluxional macrocyclic host able to form different conformations with a fine-tuned cavity because the bridging nitrogen atoms can adopt sp^2 and/or sp^3 electronic configurations and form various conjugation systems with their one and/or two adjacent pyridine rings. In the presence of a guest, **1** most likely undergoes conformation adjustment to yield a cavity structure for maximum, efficient interaction with the guest through intermolecular hydrogen-bond formation and, in some cases, C–H···π or π–π interactions.

For the complexation of **3**, for example, **1** preorganized into a slightly twisted 1,3-alternate conformation in which the distance of two hydrogen-bond acceptors (d(N(4)···N(4A))) was 4.530 Å and the cavity (d(C(4)···C(4A))) was 9.084 Å. The resulting conformation allowed the host to form the strongest intermolecular hydrogen bonds with guest **3**, as the distance between two hydroxy groups in **3** (d(O(1)···O(1A))) is 4.772 Å, very close to the distance between two hydrogen-bond acceptors. As the distance between the two hydroxy groups in **4**

 © 2007 Wiley-VCH Verlag GmbH & Co. KGaA, Weinheim

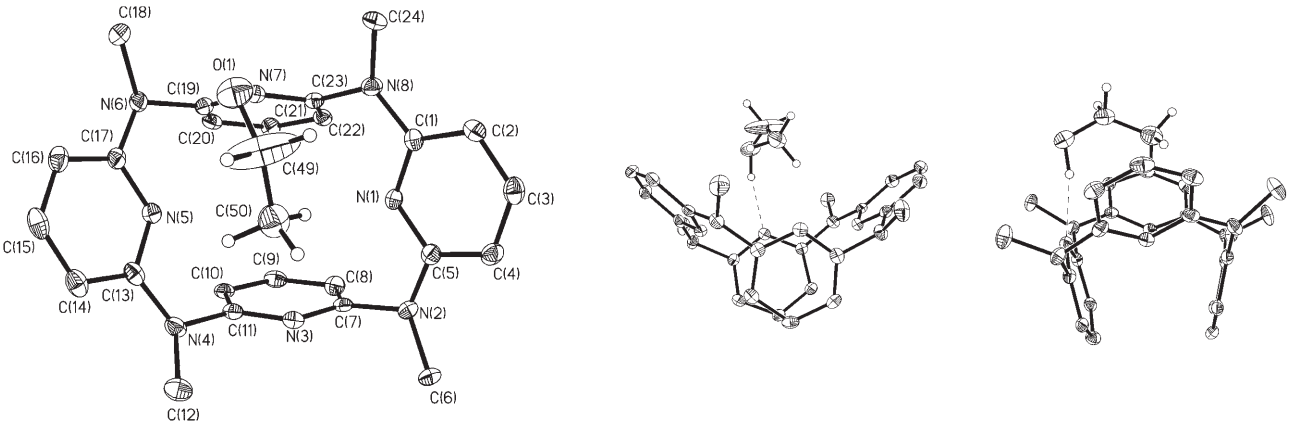

Figure 8. Molecular structure of MACP-4·ethanol complex **1·9**. Only one complex structure in the crystallographic cell is shown. Left: top view; middle and right: side view. Selected interatomic distances [Å]: N(3)···N(7) 4.630, C(9)···C(21) 3.342, N(1)···N(5) 4.853, C(3)···C(15) 8.968, N(1)···N(3) 3.170, N(3)···N(5) 3.567, N(5)···N(7) 3.172, N(7)···N(1) 3.498. Selected bond lengths [Å]: C(5)-N(2) 1.388, N(2)−C(7) 1.430, C(11)−N(4) 1.436, N(4)−C(13) 1.395, C(17)−N(6) 1.396, N(6)−C(19) 1.449, C(23)−N(8) 1.430, N(8)−C(1) 1.390, N(5)−HC(C50) 2.961, O(1)−N(7) 2.900, N(1)−HB(C50) 2.701. Selected bond angle [°]: O(1)-H(1)-N(7) 155.68.

(d(O(1)···O(1A))) is 5.501 Å, much longer than the fine-tunable distance between two hydrogen-bond receptors, the formation of two intermolecular hydrogen bonds with two isolated pyridine nitrogen atoms in **1** is not favorable. In other words, the geometry or the orientation of the two hydroxy groups in **4** prohibited the formation of two hydrogen bonds with one molecule of **1**, as was observed in the MACP-4·resorcinol complex (**1·3**). As a consequence, 1:1 complexation between **1** and **4** was not affected. Instead, two molecules of **1** interacted with one molecule of **4** by forming two strong intermolecular hydrogen bonds, thus yielding a capsule-like 2:1 complex during the crystallization. In the solid state, the formation of 1:1 complex between **1** and **2** was not a favorable process, because the distance between the two hydrogen-bond donors in **2** was 2.710 Å, too short to fine-tune as a result of the distance between two pyridine nitrogen atoms within the host. The formation of a 2:1 complex between **1** and **2**, similar to the complexation between **1** and **4**, was not energetically favored either, as such a 2:1 complexation would generate steric repulsion between two host molecules owing to the proximity of the two hydroxy groups in the guest **2**. To achieve effective interaction with **2**, **1** then smartly adjusted its structure to give a slightly twisted 1,3-alternate conformation with the largest cavity or cleft (d(C(10)···C(10A)) 9.921 Å). The wide cleft that resulted was best fit to an intermolecularly hydrogen-bonded dimer of **2**. In such a perfect complimentary structure, both the intermolecular hydrogen bonding and the π–π stacking interactions between the host and guest species were maximized.

The self-regulated fine-tunable cavity of **1** was further reflected in complexation with **5**, **6**, and **9**. In each case, the host **1** adopted a 1,3-alternate conformation with a smaller cavity size, thus allowing the formation of C−H···π interactions with the guest in addition to the intermolecular hydrogen-bonding effect.

Careful scrutiny of the hydrogen-bond lengths and angles in the molecular structures of all the complexes provides very useful information about the strength of the hydrogen bonding. The strongest hydrogen-bonding effect was seen in complex **1·3**, as evidenced by the shortest hydrogen-bond length (d(O−H···N) 2.748 Å) and large hydrogen-bond angle (∢O−H···N 177.05°). There was effective hydrogen bonding in complexes **1·5** and **1·9** as the bond lengths (d(O−H···N)) and bond angles (∢O−H···N) were 2.921–3.060 Å and 132.60–173.58°, respectively. In the case of the 1:1 complex between **1** and **6**, although the host formed two hydrogen bonds with the guest, one of the hydrogen bonds was weak with a distance of 3.132–3.133 Å. In other words, one of the hydroxy groups of 1,3-propanediol in the complex tended to leave the cavity of MACP-4. Nevertheless, the C−H···π interaction offered by the host towards the guest provided extra energy to stabilize the complexations of **1** with **5**, **6**, and **9**. It is apparently the intrinsic nature of the nitrogen-bridged calix[4]pyridine **1**, that is, the properties of the self-regulating fine-tunable cavity as a result of the electronic effects of all the bridging nitrogen atoms and the complementarity between the host and guest in terms of steric and electronic effects (i.e., the intermolecular hydrogen-bonding, C−H···π, and π···π interactions), that most probably provides the main driving force to form various isolable complexes in the solid state.

The X-ray single-crystal molecular structures showed the physical forces needed to complex the host and guest at molecular level. The interaction between the host and guest in the solid state, however, may not correlate with the host–guest association in the solution phase because of the solvation and desolvation effects in the process of molecular recognition in solution. The two strong hydrogen bonds observed between MACP-4 and resorcinol in complex **1·3** in the crystalline form seemed to be in agreement with the largest association constant ($K_a = 6000\ M^{-1}$) measured in solution. However, the comparison of the strength of the overall interactions in the complexes in the solid state did not follow the order of their association constants in solution.

 © 2007 Wiley-VCH Verlag GmbH & Co. KGaA, Weinheim

The extreme cases were the complexes of **1**·**9** and **1**·**5**, the former complex gave a larger K_a value in solution with only one hydrogen bond, whereas the latter showed a smaller K_a value but with two hydrogen bonds in the solid state. The formation of a strong 1:1 complex ($K_a = 6000\ M^{-1}$) between **1** and **3** in solution was also very intriguing.

To shed light on the mechanism of diol recognition by **1** in solution, the interactions of **1** with **3**, **4**, and **6** were further studied by variable-temperature ^{1}H NMR spectroscopic analysis. ^{1}H NMR titration of diols with **1** in solution with $CDCl_3$ was measured at 298–223 K. For the complexation of **1** with **4**, the proton signals broadened below 238 K. Based on the ^{1}H NMR titration isotherms, association constants, and therefore the free-energy changes $\Delta G°$, at different temperatures were obtained. The van't Hoff plot of $\ln K_a$ against $1/T$ (see Figure 9 and the Supporting Information)

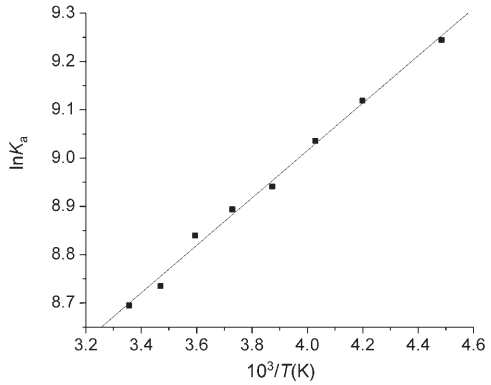

Figure 9. Plot of $\ln K_a$ versus $10^3/T$ for the complexation of **1** with **3** in $CDCl_3$.

gave enthalpy $\Delta H°$ and entropy $\Delta S°$ values. The complexation of **1** with **4** and **6** was enthalpically favorable but entropically unfavorable (Table 3). The large exothermic enthalpy value determined for the complexation of **1** with **4** and **6** was attributable to the intermolecular hydrogen-bonding and C–H···π interactions that resulted in structural tightening. Concomitantly, the structural tightening, especially the association of a linear diol **6** with one or two host molecules, led to a decrease in the entropy of the system. Noticeably, however, the binding of **1** with **3** was driven by a combination of both favorable enthalpy and entropy. The usual small enthalpy effect ($\Delta H° = -4.1\ kJ\,mol^{-1}$) and extraordinarily large positive entropic effect ($\Delta S° = 58.6\ J\,mol^{-1}\,K^{-1}$) observed for the complexation of **1** with **3** indicated a strong solvation effect of the guest in solution. In other words, the guest **3** was probably heavily solvated. The complexation of host **1** with **3**, therefore, proceeded most probably with the desolvation process and is associated with the release of solvent molecules into the bulk solution, thus leading to a large positive entropy effect. The desolvation effect also partially cancelled the enthalpy gained from the formation of two strong hydrogen bonds in complex **1**·**3**, thus giving rise to a relatively small enthalpy effect.

Table 3. Thermodynamic characteristics from ^{1}H NMR binding titrations for the formation of complexes between **1** and **3**, **4**, and **6**.

Guest	Complex	$\Delta G°_{298K}$ [kJ mol^{-1}]	$\Delta H°$ [kJ mol^{-1}]	$\Delta S°$ [J mol^{-1} K]
3	**1**·**3**	−21.5 ± 0.5	−4.1 ± 0.1	58.6 ± 0.5
4	**1**·**4**	−8.0 ± 0.1	−28.1 ± 0.3	−67.9 ± 1.2
6	**1**·**6**	−7.3 ± 0.1	−39.4 ± 0.9	−107.7 ± 3.4
6	**1**$_2$·**6**	−11.3 ± 0.3	−77.8 ± 0.9	−223.3 ± 3.4

Having established the thermodynamics of the molecular interaction of MACP-4 with diols by revealing different enthalpy and entropy contributions to free energy, we turned our attention to the dynamics of the complexation of **1** with a guest. The binding of **1** with **3** was chosen as a case study because of their strong interaction. The ^{1}H NMR spectra of **1** in solution with CD_2Cl_2 and of a mixture of **1** and **3** in the ratios of 4:1, 1:1, and 0.5:1 were recorded from 298 to 188 K (Figure 10).

Figure 10a showed that the host molecule gave only one set of proton signals in the ^{1}H NMR spectra at 298–188 K, thus clearly indicating that the conformational structures of the host **1** in solution were very flexible and the interconversions were very rapid on the NMR timescale. At 298–248 K, a mixture of **1** (4×10^{-3} M) and **3** (1×10^{-3} M) gave one set of proton signals that correspond to a 2,6-disubstituted pyridine moiety and resorcinol ring. This behavior suggested a fast equilibrium between the host **1** and complex **1**·**3** in solution above 248 K (Figure 10b). Very noticeably, when the temperature was lower than 243 K, another four broad peaks centered at $\delta = 7.29$, 7.16, 6.56, and 5.75 ppm began to emerge with the concomitance decrease in the intensity of the original pyridine proton signals. These four broad peaks became two pairs of well-resolved and mutually coupled triplets and doublets when the temperature decreased further to below 208 K. The equal intensity of these two pairs of signals, one pair downfield shifted and the other upfield shifted relative to the original pyridine proton signals, implied that they were the proton signals of two types of new pyridine moieties. The variable-temperature ^{1}H NMR spectra of a 1:1 mixture of **1** and **3** (Figure 10c) showed undoubtedly that one set of the pyridine proton signals of the MACP-4 component in the complex **1**·**3** transformed into two sets of well-resolved signals when the temperature decreased to below 208 K. This outcome convincingly indicated that at temperatures higher than 243 K the macrocyclic ring of MACP-4 in the **1**·**3** complex underwent rapid conformational interconversions, thus giving one set of pyridine proton signals on the NMR timescale. When the temperature decreased, the equilibrium between the host and the complex became slower. Furthermore, the conformation of MACP-4 in the **1**·**3** complex was frozen or rigidified, thus leading to two types of nonequivalent pyridine rings that gave two sets of pyridine proton signals of equal intensity. The stable complex structure in solution at low temperature was also evidenced by the strong NOE interaction signals

 © 2007 Wiley-VCH Verlag GmbH & Co. KGaA, Weinheim

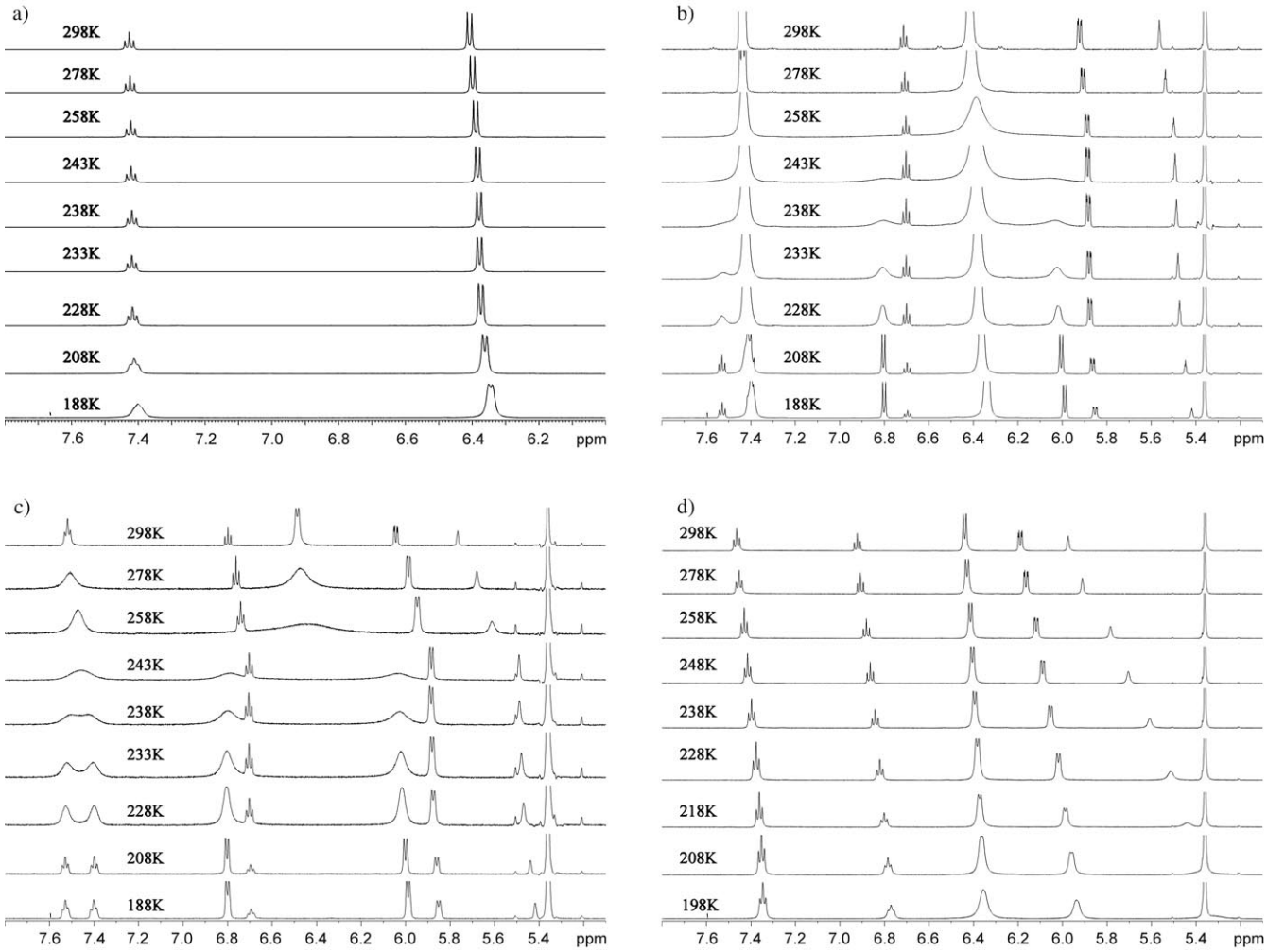

Figure 10. The partial variable-temperature ^{1}H NMR spectra of **1** in solution with CD_2Cl_2 ([**1**] = 1×10^{-3} M). Mixtures of **1** and **3** in ratios of a) 4:1, b) 1:1, and c) 0.5:1. d) The concentration of **3** was kept constant as 1×10^{-3} M.

between the host and guest, as revealed by the NOESY spectra at 198 K (Figure 11), which is similar to that in the solid state (see below). It was very interesting to note that in contrast to the equilibrium between the MACP-4 host and complex **1**·**3**, which was strongly influenced by the temperature, the equilibrium between the guest **3** and complex **1**·**3** and between the conformers of the complex were rather rapid. This behavior was exemplified by the observation of only one set of proton resonance signals of pyridine and resorcinol when the ^{1}H NMR spectra of a 0.5:1 mixture of **1** and **3** in CD_2Cl_2 were recorded at 298–198 K (Figure 10d).

The process of conformational changes in both the host molecule **1** and the host–guest complex **1**·**3** in solution can be treated as a two-site exchange model from the viewpoint of a dynamic NMR spectroscopic study.[18] Based on the variable-temperature ^{1}H NMR spectra (Figure 10), kinetic parameters (Table 4) for the formation of complex **1**·**3** and the conformational inversion of the macrocyclic ring of **1** and complex **1**·**3** were calculated (see the Supporting Information) following reported methods.[19] Combined with the free-energy $\Delta G°_{243\,K}$ value obtained previously (Figure 9 and Table 3), the potential-energy profiles of the processes, including the complexation of MACP-4 with resorcinol and the conformational inversions, are shown in Figure 12. The activation energy $\Delta G°_{243\,K}$ for the formation of complex **1**·**3** is (55.3 ± 0.3) kJ mol^{-1}. The inversion of the conformation of **1** in the absence of a guest molecule requires an activation energy of $\Delta G°_{243\,K} = (33.2\pm0.7)$ kJ mol^{-1}, whereas an activation energy of $\Delta G°_{243\,K} = (45.5\pm2.2)$ kJ mol^{-1} is needed when an equal and an excess amount of host is present for the conformational inversion of the tetramethylazacalix[4]pyridine ring of its resorcinol complex **1**·**3**. In presence of an excess amount of **3**, a decreased activation energy $\Delta G°_{243\,K} = (33.5\pm1.5)$ kJ mol^{-1} can affect the inversion of the conformation of the host of complex **1**·**3**. Such an acceleration of the inversion of the conformation most probably stems from the tendency of the nonbonded pyridine nitrogen atoms of the **1**·**3** complex to interact with the two hydroxy groups of free **3** present in the solution. In other words, it was most likely that the very rapid equilibrium between the **1**·**3** com-

 © 2007 Wiley-VCH Verlag GmbH & Co. KGaA, Weinheim

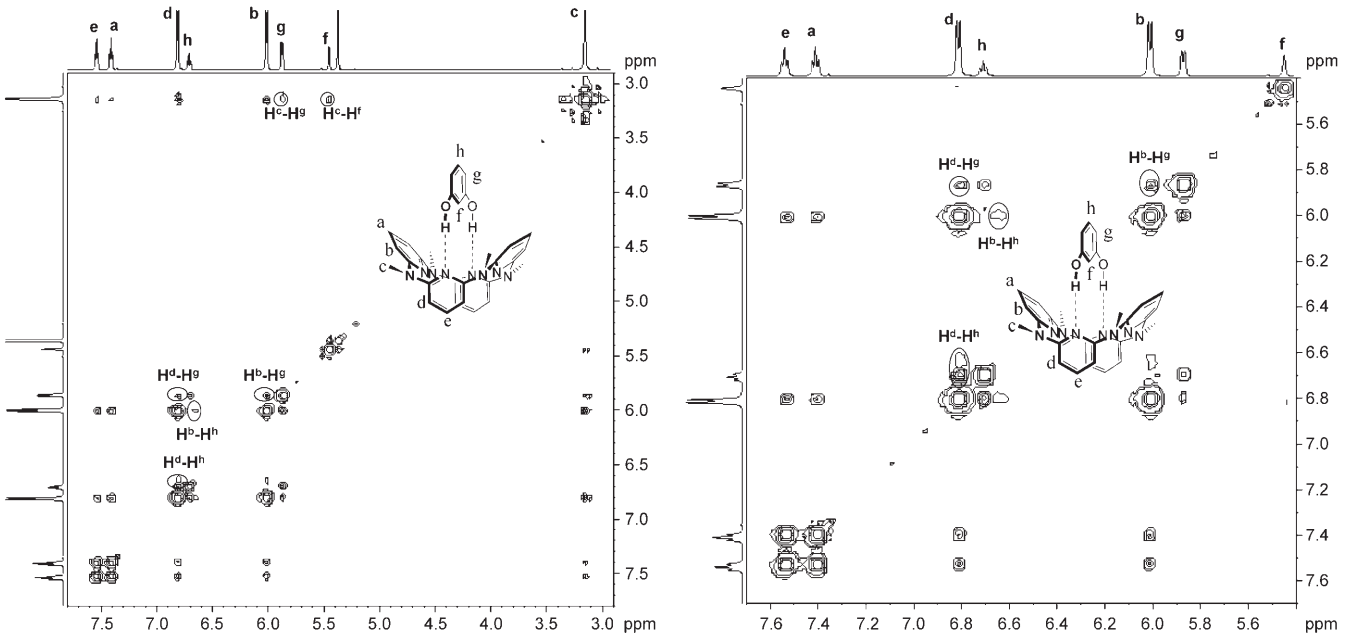

Figure 11. The partial NOESY spectra of a mixture of **1** and **3** (1:1) in solution with CD_2Cl_2 ($[\mathbf{1}]=1\times10^{-3}$ M, $[\mathbf{3}]=1\times10^{-3}$ M) at 198 K.

Table 4. Kinetic parameters for conformational change in complex **1**·**3** at 243 K

Entry	Process	$\Delta H°$ [kJ mol^{-1}]	$\Delta S°$ [J K^{-1} mol^{-1}]	$\Delta G°$ [kJ mol^{-1}]
1	conformation inversion of **1**	14.0±0.3	−77.2±1.6	33.2±0.7
2	**1**→**1**·**3**	−5.3±0.1	−244.0±0.7	55.3±0.3
3	conformation inversion of **1**·**3** (in the presence of an equal or excess amount of **1**)	42.5±1.1	−12.1±4.4	45.5±2.2
4	conformation inversion of **1**·**3** (in the presence of an excess amount of **3**)	23.8±0.7	−39.1±3.0	33.5±1.5

plex and **3** proceeded through the $[\mathbf{3}\cdots\mathbf{1}\cdots\mathbf{3}]^{\neq}$ transition state (Figure 12), which is very similar to the mechanism of a S_N2 reaction.

Conclusion

In summary, we have shown that methylazacalix[4]pyridine (**1**) is a unique macrocyclic host that is able to form various guest-dependent host–guest complexes with diols in both solution and the solid state. Whereas **1** forms 2:1 complexes with aliphatic diols, such as ethylene glycol (**5**), 1,3-propanediol (**6**), and 1,4-butylene glycol (**7**), 1:1 complexes result from the interaction of **1** with aromatic diols, such as catechol (**2**), resorcinol (**3**), and hydroquinone (**4**), in solution. In the solid state, the complexation of **1** with **3**, **5**, or **6** affords a stable sandwich-like 1:1 complex, whereas a capsule-like 2:1 complex and a butterfly-layered 1:2 complex are obtained from the interaction of **1** with **4** and **2**, respectively. The predominant driving force for the formation of complexes between **1** and diols is the intermolecular hydrogen bonding between the pyridine nitrogen atoms of the host and the hydroxy groups of the guest, although C–H···π and π–π interactions also contribute in the case of complexes **1** of with aliphatic diols **5** and **6** and aromatic diol **2**, respectively.

The ability of **1** to form various complexes with diols of different structures and geometries originates from its intrinsic electronic and steric features. As a macrocycle, **1** undergoes conformational inversions very rapidly in solution. In the presence of a diol guest, **1** can most likely self-regulate its conformation through the formation of slightly different conjugations of the four bridging nitrogen atoms with their adjacent pyridine rings to form a cavity to best fit the guest species. Because of the pro-organization of the two hydrogen-bond acceptors of the two face-to-face parallel pyridine moieties and the cleft resulting from two edge-to-edge oriented 2,6-diaminopyridine segments, and because of the favorable enthalpy and entropy effects, **1** exhibits the strongest bonding affinity towards **3** by forming a 1:1 complex with a binding constant of 6000 M^{-1}. The large difference in binding affinities of **1** towards various diols and monools render it a useful host. The application of **1** in the selective recognition of **3** is demonstrated in Figure 13, in which the addition of **1** into a mixture of isomeric benzene diols led remarkably to the upfield shift of the aromatic protons of **3** in contrast to the lack of all the proton resonance signals corresponding to **2** and **4** in the ^{1}H NMR spectra.

The dynamic ^{1}H NMR spectroscopic study showed that **1** undergoes conformational inversion very rapidly with an ac-

 © 2007 Wiley-VCH Verlag GmbH & Co. KGaA, Weinheim

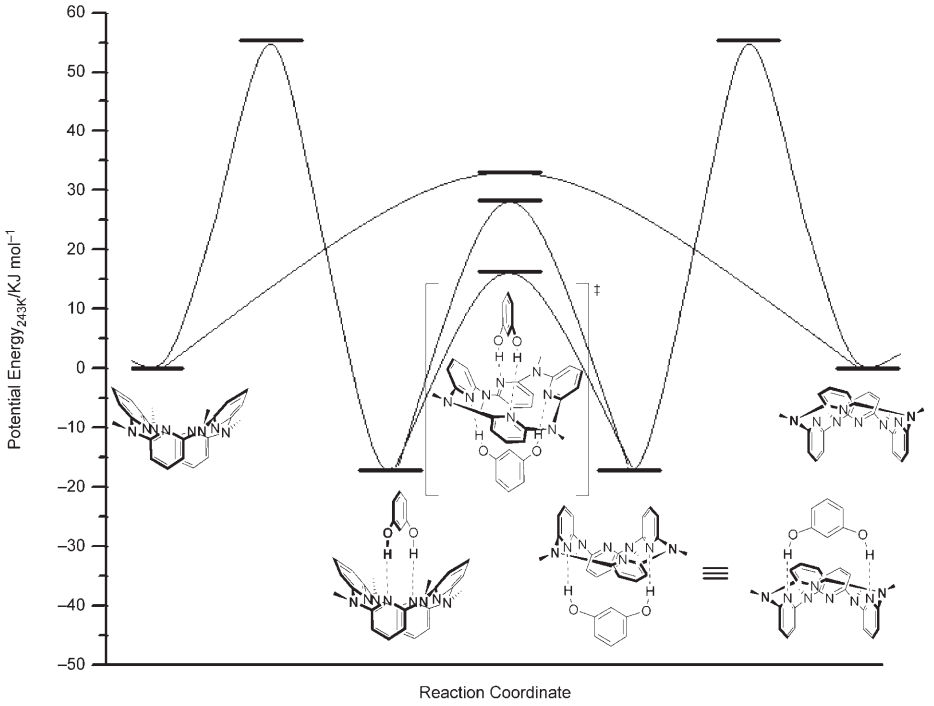

Figure 12. The potential-energy diagram for the formation of MACP-4·resorcinol complex **1·3** and the inversion of the conformation of the host **1** and the host–guest complex **1·3** at 243 K relative to **1**.

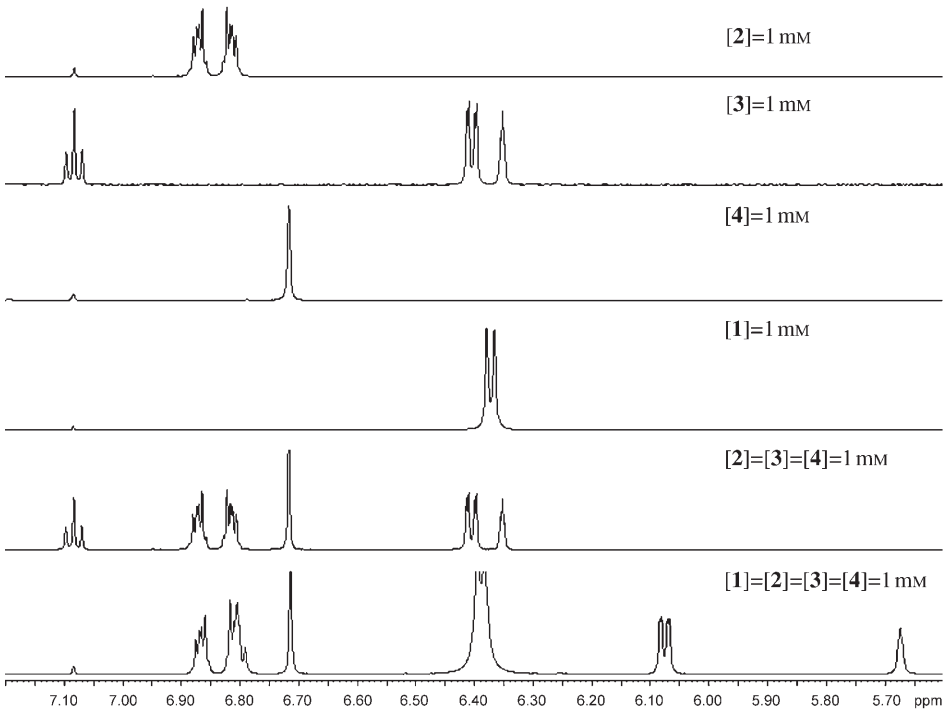

Figure 13. Selective recognition of **3** by **1** in the presence of **2** and **4**. Partial ^{1}H NMR spectra at 298 K.

tivation energy of $\Delta G°_{243\,K} = (33.2 \pm 0.7)$ kJ mol^{-1}. The 1,3-alternate conformation of the macrocyclic ring of **1** of the MACP-4·resorcinol complex (**1·3**) is stable at temperatures lower than 243 K, and its conformational inversion requires a larger activation energy ($\Delta G° = (45.5 \pm 2.2)$ kJ mol^{-1}). In the presence of an excess amount of **3**, however, the inversion of the conformation of complex **1·3** proceeds more readily with a decreased activation energy ($\Delta G° = (33.5 \pm 1.5)$ kJ mol^{-1}) owing most probably to the favorable enthalpy effect of the $[\mathbf{3}\cdots\mathbf{1}\cdots\mathbf{3}]^{\neq}$ transition state.

Experimental Section

Methylazacalix[4]pyridine (**1**) was synthesized from a step-wise cross-coupling approach starting from 2,6-dibromopyridine and 2,6-diaminopyridine derivatives.[10e] The interaction between the macrocyclic host molecule and alcohol guest species in solution was studied by means of ^{1}H NMR titrations at varying temperatures. In each binding experiment, the diol concentration was kept constant and the concentration of **1** was increased gradually from 0 to 2.316×10^{-2} M. The stoichiometry of the complex between the host and guest species was obtained by the Job plot method, or in some cases by a nonlinear least-squares fit method.[16] The binding constants for the complexation of **1** with guest molecules were calculated on the basis of ^{1}H NMR experimental isotherms using the Hyperquad2003 program.[17] The solid-phase interaction between the host and guest species was investigated by single-crystal X-ray crystallographic studies. Single crystals of complexes between **1** and **2**–**4** were obtained by slow evaporation of the solvent at 283 K from a solution of **1** (10 mg) and **2**, **3**, or **4** (20 mg) in a mixture of CH_2Cl_2 and CH_3OH (v/v = 5:1). Single crystals of the complexes between **1** and **5**, **6**, **8**, and **9** were obtained by slow evaporation of the solvent at 283 K from a solution of **1** (10 mg) in a mixture of **5**, **6**, **8**, or **9** and CH_2Cl_2 (v/v = 1:10). The X-ray crystallographic data are summarized in Table 1. The kinetic parameters were calculated from the dynamic ^{1}H NMR spectroscopic data using a two-site exchange model (see the Supporting Information).[18,19]

 © 2007 Wiley-VCH Verlag GmbH & Co. KGaA, Weinheim

Acknowledgements

We thank the National Natural Science Foundation of China, Ministry of Science and Technology, and the Chinese Academy of Sciences for financial support. We also thank Prof. Y.-L. Wang and Dr. H.-W. Ma for helpful discussions.

[1] a) *Comprehensive Supramolecular Chemistry, Vols. 1 and 2* (Eds.: J. L. Atwood, J. E. D. Davies, D. D. MacNicol, F. Vogtle), Pergamon, Elsevier Science, **1996**; b) *Anion Sensing in Topics in Current Chemistry, Vol. 255* (Ed.: I. Stibor), Springer, Heidelberg, **2005**.

[2] a) For a recent useful overview, see: S. L. Wiskur, J. J. Lavigne, A. Metzger, S. L. Tobey, V. Lynch, E. V. Anslyn, *Chem. Eur. J.* **2004**, *10*, 3792; b) G. Springsteen, B. Wang, *Tetrahedron* **2002**, *58*, 5291 and references therein.

[3] Y. Kikuchi, Y. Kato, Y. Tanaka, H. Toi, Y. Aoyama, *J. Am. Chem. Soc.* **1991**, *113*, 1349.

[4] C.-Y. Huang, L. A. Cabell, E. V. Anslyn, *J. Am. Chem. Soc.* **1994**, *116*, 2778.

[5] Y. Dobashi, A. Dobashi, H. Ochiai, S. Hara, *J. Am. Chem. Soc.* **1990**, *112*, 6121.

[6] S. Hanessian, M. Simard, S. Roelens, *J. Am. Chem. Soc.* **1995**, *117*, 7630.

[7] For a useful overview of heteroatom-bridged calixarenes, see: B. König, M. H. Fonseca, *Eur. J. Inorg. Chem.* **2000**, 2303.

[8] For a very recent review on thiacalixarenes, see: N. Morohashi, F. Narumi, N. Iki, T. Hattori, S. Miyano, *Chem. Rev.* **2006**, *106*, 5291.

[9] For recent examples of oxygen-bridged calix aromatic compounds, see: a) M.-X. Wang, H.-B. Yang, *J. Am. Chem. Soc.* **2004**, *126*, 15412; b) J. L. Katz, M. B. Feldman, R. R. Conry, *Org. Lett.* **2005**, *7*, 91; c) J. L. Katz, K. J. Selby, R. R. Conry, *Org. Lett.* **2005**, *7*, 3505; d) J. L. Katz, B. J. Geller, R. R. Conry, *Org. Lett.* **2006**, *8*, 2755; e) W. Maes, W. Van Rossom, K. Van Hecke, L. Van Meervelt, W. Dehaen, *Org. Lett.* **2006**, *8*, 4161; f) E. Hao, F. R. Fronczek, M. G. H. Vicente, *J. Org. Chem.* **2006**, *71*, 1233; g) R. D. Chambers, P. R. Hoskin, A. R. Kenwright, A. Khalil, P. Richmond, G. Sandford, D. S. Yufit, J. A. K. Howard, *Org. Biomol. Chem.* **2003**, *1*, 2137; h) R. D. Chambers, P. R. Hoskin, A. Khalil, P. Richmond, G. Sandford, D. S. Yufit, J. A. K. Howard, *J. Fluorine Chem.* **2002**, *116*, 19; i) X. H. Li, T. G. Upton, C. L. D. Gibb, B. C. Gibb, *J. Am. Chem. Soc.* **2003**, *125*, 650; j) F. Yang, L.-W. Yan, K.-Y. Ma, L. Yang, J.-H. Li, L.-J. Chen, J.-S. You, *Eur. J. Org. Chem.* **2006**, 1109; k) Q.-Q. Wang, D.-X. Wang, H.-W. Ma, M.-X. Wang, *Org. Lett.* **2006**, *8*, 5967.

[10] For recent examples of nitrogen-bridged calixaromatics, see: a) A. Ito, Y. Ono, K. Tanaka, *New J. Chem.* **1998**, *22,* 779; b) A. Ito, Y. Ono, K. Tanaka, *J. Org. Chem.* **1999**, *64*, 8236; c) Miyazaki, T. Kanbara, T. Yamamoto, *Tetrahedron Lett.* **2002**, *43*, 7945; d) M.-X. Wang, X.-H. Zhang, Q.-Y. Zheng, *Angew. Chem.* **2004**, *116*, 856; *Angew. Chem. Int. Ed.* **2004**, *43*, 838; e) H.-Y. Gong, X.-H. Zhang, D.-X. Wang, H.-W. Ma, Q.-Y. Zheng, M.-X. Wang, *Chem. Eur. J.* **2006**, *12*, 9262; f) H.-Y. Gong, Q.-Y. Zheng, X.-H. Zhang, D.-X. Wang, M.-X. Wang, *Org. Lett.* **2006**, *8*, 4895; g) H. Tsue, K. Ishibashi, H. Takahashi, R. Tamura, *Org. Lett.* **2005**, *7*, 11; h) W. Fukushima, T. Kanbara, T. Yamamoto, *Synlett* **2005**, 2931; i) T. D. Selby, S. C. Blackstock, *Org. Lett.* **1999**, *1*, 2053; j) Y. Suzuki, T. Yanagi, T. Kanbara, T. Yamamoto, *Synlett* **2005**, 263; k) K. Ishibashi, H. Tsue, S. Tokita, K. Matsui, H. Takahashi, R. Tamura, *Org. Lett.* **2006**, *8*, 5991.

[11] For examples of other heteroatom/bridged calix aromatic compounds, see: a) B. König, M. Rödel, P. Bubenitschek, P. G. Jones, I. Thondorf, *J. Org. Chem.* **1995**, *60*, 7406; b) B. König, M. Rödel, P. Bubenitschek, P. G. Jones, *Angew. Chem.* **1995**, *107*, 752; *Angew. Chem. Int. Ed. Engl.* **1995**, *34*, 661. ; c) M. Yoshida, M. Goto, F. Nakanishi, *Organometallics* **1999**, *18*, 1465; d) N. Avarvari, N. Mezailles, L. Ricard, P. Le Floch, F. Mathey, *Science*, **1998**, *280*, 1587; e) N. Avarvari, N. Maigrot, L. Ricard, F. Mathey, P. Le Floch, *Chem. Eur. J.* **1999**, *5*, 2109.

[12] a) C. D. Gutsche, *Calixarenes*, The Royal Society of Chemistry, Cambridge, **1989**; b) C. D. Gutsche, *Calixarenes Revisited*, The Royal Society of Chemistry, Cambridge, **1998**; c) *Calixarenes in Action* (Eds.: L. Mandolini, R. Ungaro), Imperial College Press, London, **2000**; d) *Calixarenes 2001* (Eds.: Z. Asfari, V. Böhmer, J. Harrowfield, J. Vicens, M. Saadioui), Kluwer Academic Publishers, The Netherlands, **2001**.

[13] For reviews of calixpyrroles, see: a) P. A. Gale, P. Anzenbacher, J. L. Sessler, *Coord. Chem. Rev.* **2001**, *222*, 57; b) W. Sliwa, *Heterocycles* **2002**, *57*, 169.

[14] For examples of calixpyridines, see: a) V. Král, P. A. Gale, P. Anzenbacher, K. Jursiková, V. Lynch, J. L. Sessler, *Chem. Commun.* **1998**, 9; b) J. L. Sessler, W.-S. Cho, V. Lynch, V. Král, *Chem. Eur. J.* **2002**, *8*, 1134; c) G. R. Newkome, Y. J. Joo, F. R. Fronczek, *J. Chem. Soc. Chem. Commun.* **1987**, 854.

[15] For recent examples of other calix(hetero) aromatic compounds, see: a) J. Guillard, O. Meth-Cohn, C. W. Rees, A. J. P. White, D. J. Williams, *Chem. Commun.* **2002**, 232; b) E. Vogel, M. Pohl, A. Herrmann, T. Wiss, C. König, J. Lex, M. Gross, J. P. Gisselbrecht, *Angew. Chem.* **1996**, *108*, 1677; *Angew. Chem. Int. Ed. Engl.* **1996**, *35*, 1520; c) D. S. Black, D. C. Craig, R. Rezaie, *Chem. Commun.* **2002**, 810; d) J. L. Sessler, W.-S. Cho, V. Lynch, V. Král, *Chem. Eur. J.* **2002**, *8*, 1134; e) G. Cafeo, F. H. Kohnke, G. L. La Torre, A. J. P. White, D. J. Williams, *Angew. Chem.* **2000**, *112*, 1556; *Angew. Chem. Int. Ed.* **2000**, *39*, 1496; ; f) G. Cafeo, F. H. Kohnke, G. L. La Torre, M. F. Parisi, R. P. Nascone, A. J. P. White, D. J. Williams, *Chem. Eur. J.* **2002**, *8*, 3148; g) G. Cafeo, D. Garozzo, F. H. Kohnke, S. Pappalardo, M. F. Parisi, R. P. Nascone, D. J. Williams, *Tetrahedron* **2004**, *60*, 1895; h) S. Kumar, D. Paul, H. Singh, *Adv. Heterocycl. Chem.* **2005**, *89*, 65.

[16] J. Bourson, J. Pouget, B. Valeur, *J. Phys. Chem.* **1993**, *97*, 4552.

[17] a) P. Gans, A. Sabatini, A. Vacca, *Talanta* **1996**, *43*, 1739; b) Hyperquad2003 software, Protonic Software, http://www.hyperquad.co.uk.

[18] a) J. Sandström, *Dynamic NMR Spectroscopy*, Academic, London, **1982**; b) H. Friebolin, *Basic One- and Two-Dimensional NMR Spectroscopy*, Wiley-VCH, Weinheim, **2005**; c) M. Ôki, *Applications of Dynamic NMR Spectroscopy to Organic Chemistry*, VCH, Weinheim, **1985**.

[19] a) H. S. Gutowsky, C. H. Holm, *J. Chem. Phys.* **1956**, *25*, 1228; b) A. Allerhand, H. S. Gutowsky, J. Jonas, R. A. Meinzer, *J. Am. Chem. Soc.* **1966**, *88*, 3185; c) L. H. Piette, W. A. Anderson, *J. Chem. Phys.* **1959**, *30*, 899; d) H. Shanan-Atidi, K. H. Bar-Eli, *J. Phys. Chem.* **1970**, *74*, 961.

Received: March 30, 2007
Published online: June 21, 2007

 © 2007 Wiley-VCH Verlag GmbH & Co. KGaA, Weinheim